THE INFLUENCE OF TEMPERATURE AND SURFACE STRUCTURE ON THE FRICTION OF DYNAMIC HYDRAULIC SEALS
Numerical and Experimental Investigations

Julian ANGERHAUSEN[*], Hubertus MURRENHOFF[*], Leonid DOROGIN[**], Bo N. J. PERSSON[**], Michele SCARAGGI[***]

[*] Institute for Fluid Power Drives and Controls (IFAS)
RWTH Aachen University
Steinbachstraße 53, 52074 Aachen, Germany
(E-mail: Julian.Angerhausen@ifas.rwth-aachen.de)
[**] Peter Grünberg Institut – 1
Forschungszentrum Jülich
Leo-Brandt-Straße, 52428 Jülich, Germany
[***] Dipartimento di Ingegneria dell'Innovazione
Università del Salento
Centro Ecotekne Pal. O-S.P. 6, 73047 Monteroni (Lecce), Italy

Abstract. Seals are crucial machine elements in hydraulic devices. A seal failure can result in expensive production downtimes or even environmentally hazardous leakage. However, especially in regard to dynamic seals - for example in cylinder applications - the physical understanding of the sealing mechanism is still insufficient. A test rig and a transient, finite element (FE) based elastohydrodynamic (EHD) simulation for translational hydraulic seals have been set up to investigate a soft, lubricated line contact in detail. In this paper the influences of temperature and surface structure on the friction force is investigated numerically and experimentally. The focus is upon the mixed friction regime as - especially during a change in the cylinder stroke's direction - solid body friction and fluid friction occur in the tribological contact between seal and cylinder surface.

Keywords: Dynamic Seals; Transient Simulation; Friction; Surface; Temperature

INTRODUCTION

Research on elastomeric seals dates back to the 1930s and 1940s [1]. Still, the theoretical understanding of the sealing mechanism, especially in regard to dynamic seals - for example in hydraulic cylinder applications - is insufficient. In the manufacturing process of hydraulic cylinders numerous surface finishing methods such as coating, grinding or polishing are used, provoking diverse rough and anisotropic surface topographies. This surface topography has a significant influence on the sealing system regarding leakage and friction [2]. The practical design and optimization process of translational hydraulic seals is often supported by stationary finite element (FE) calculations [3]. Here the influence of the fluid film and especially of different surface topographies is usually neglected. For basic calculations of the fluid film Blok's inverse hydrodynamic lubrication (IHL) theory [4] is often applied, where a perfectly smooth surface is assumed and any solid contact is neglected. In order to take the solid contact into account the direct method is applied [5]. For the simulation of hydraulic seals in general an upstream FE simulation is performed in order to calculate the macroscopic deformation and the resulting pressure between the mating surfaces ([6], [7], [8], [9]). Effects of the surface roughness, roughness profiles and roughness orientations can be implemented using the concept of flow factors, developed by Patir and Cheng (1978) [10]. Based on this concept a methodology that includes the influence of a micro-patterned rod was presented by Huang and Salant (2014) [11]. Wohlers et al. (2010) investigated the effect of surface roughness on the friction behaviour of step seals in a computational study [12]. They applied Persson's contact theory in their calculations, but any transient effects were neglected [13].
The approach present in this paper is based on a concept of Öngün [14], [15] and Schmidt [16]. The fluid film calculations are directly implemented into a dynamic FE calculation within the software ABAQUS. We additionally coupled the FE calculation with Persson's contact theory in order to achieve a physically based, transient model. In this paper the implementation and the influences of surface structure effects and temperature are presented. First the simulation model is described. Afterwards simulation results are presented and compared to measured friction forces for different surfaces and temperatures.

SIMULATION MODEL

A schematic view of the investigated contact problem is shown in figure 1. A seal is squeezed against a (hard, rough) rod surface with a normal load F_L. The coordinate system is introduced with the x-axis along the sliding direction, whereas the y-axis corresponds to the gap height, that is the distance orthogonal to the rigid rod surface. The boundary surface is fixed in x-direction. The normal Forces F_N and the tangential forces F_T are acting on the seal surface in the contact area. In the mixed friction regime theses forces are the sum of solid contact and fluid contact forces.

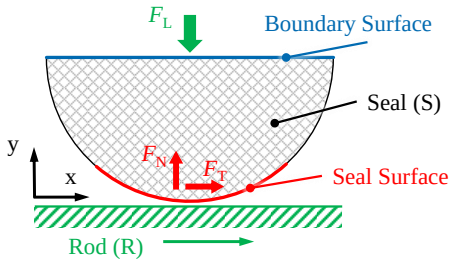

FIGURE 1. Schematic of the investigated contact

The structure of the simulation is illustrated in figure 2. Both solid and fluid interaction, and the influence of the friction force are considered in the calculation of the seal's deformation. The deformation is not only influenced by the friction forces, the solid and fluid contact, but also affects them. Thus, a strongly coupled model is introduced. The following section focusses on the implementation of temperature and surface structure influences. A detailed description of the underlying model can be found in [17].

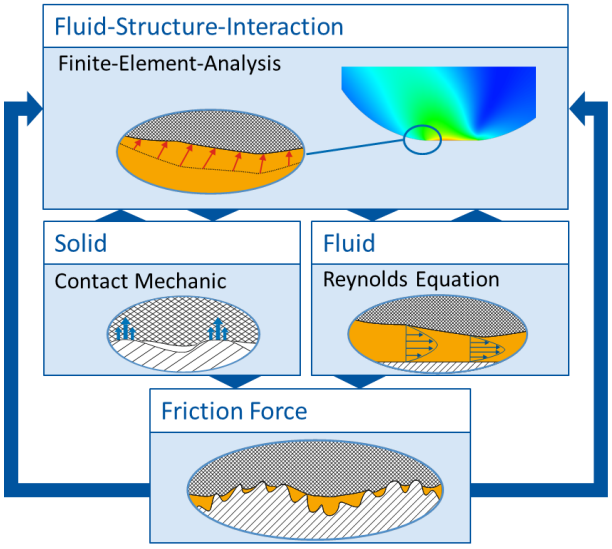

FIGURE 2. Structure of the EHD-simulation model

Deformation of the Seal

The deformation of the seal is calculated in a dynamic finite element (FE) simulation using ABAQUS [18]. Hyper- and viscoelastic material properties are taken into account in order to model the static and dynamic behaviour of the material at different frequencies and temperatures. For the computation of the temperature dependent behaviour the Williams-Landel-Ferry (WLF) approximation is applied [19]. Here the viscoelastic material data is shifted by a factor a_ϑ (eq. 1) to higher or lower frequencies, depending on the temperature ϑ. On the left side of figure 3 the measured E-Modulus (storage part) of the rubber at different temperatures and the corresponding master curve (at 20 °C) are shown. The correlation of frequency and temperature is quite distinct. The parameters A and B (here: $A = 25.61$, $B = 250$ °C) of the WLF equation are optimized based on experimental data of the elastomer. A comparison of the measured and the model time shift is shown on the right in figure 3.

$$\lg(a_\vartheta) = -A\frac{\vartheta-\vartheta_G}{B+\vartheta-\vartheta_G} \quad (1)$$

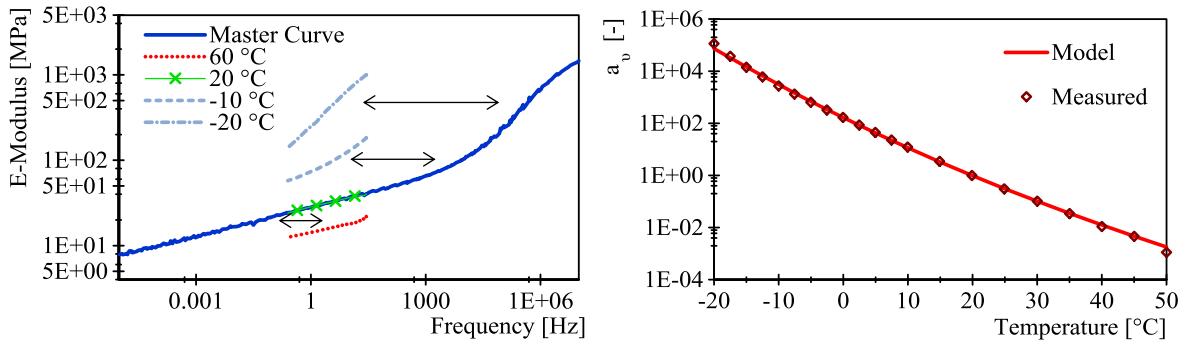

FIGURE 3. Left: E-Modulus of the NBR as function of frequency (measured curves at selected temperatures and resulting master curve); Right: Temperature shift factor for the rubber material

Fluid Film Calculation

For the numerical calculation of the fluid film and its influences on the seal deformation, the FE simulation is coupled with an implementation of the transient Reynold's equation (2), using user subroutines as suggested by [2] and [3].

$$\frac{\partial}{\partial x}\left(\Phi^P \frac{h^3}{12\eta}\frac{\partial p}{\partial x}\right) = \frac{\partial}{\partial x}\left(\frac{h\, v_x}{2}\right) - \frac{\partial}{\partial x}\left(\frac{v_x}{2} R_q \Phi^\tau\right) + \frac{\partial h}{\partial t} \quad (2)$$

Besides the gap height h, the relative velocity v_x and the oil dynamic viscosity η, two correction factors are included in this form of the Reynold's equation, namely Φ^P(pressure flow factor) and Φ^τ (shear flow factor), based on the concept of Patir and Cheng [10]. These factors are determined by the surface topographies of the mating surfaces.

The assumed influence of the surface topography on the fluid film is shown schematically in figure 4. On the left side the surface is ground in the direction of motion. The fluid is expected to flow easily through the ground channels and the fluid pressure build-up is reduced. On the other hand, when the surface is ground orthogonal to the direction of motion, as shown on the right side, the fluid is assumed to be trapped in the groves and the fluid pressure build-up is increased. This exemplification holds, when the grooves are smaller than the smallest nominal contact length [2].

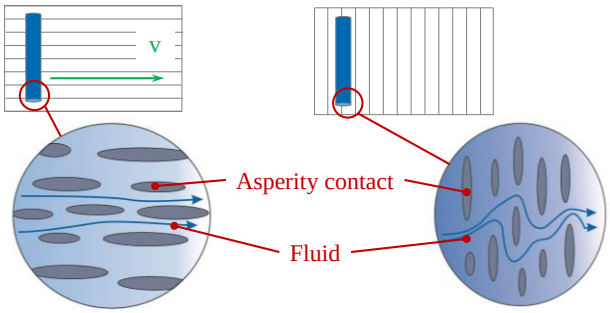

FIGURE 4. Influence of the surface topography on the fluid film (left: surface is ground in the direction of motion; right: surface is ground orthogonal to the direction of motion)

The exact calculation of the flow factors is shown in [20]. In figure 5 the flow factors for three investigated surfaces are shown. While one surface (dotted line) is stochastically, isotopically rough (sandblasted), the topography of the other surfaces is anisotopically (ground in or orthogonal to the direction of motion).

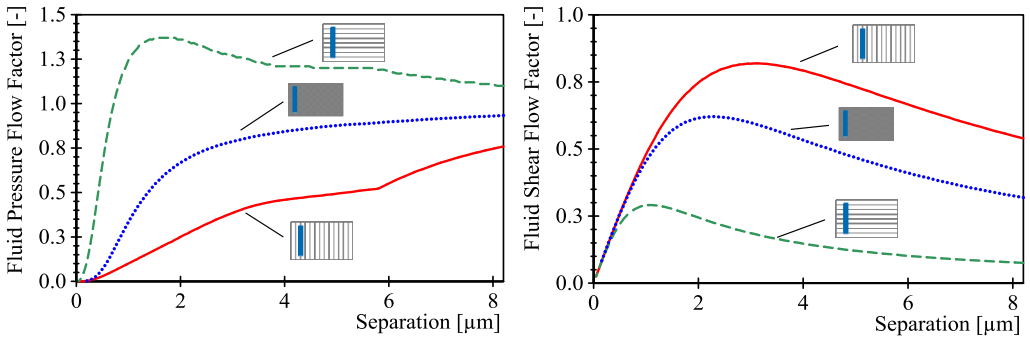

FIGURE 5. Flow factors as a function of the gap height for three different surface topographies

For the calculation of the oil viscosity and density the model of Witt [21] is applied. A comparison of the measured and the calculated oil viscosity and density is shown in figure 6. The pressure dependency of the oil parameters is neglected in this study.

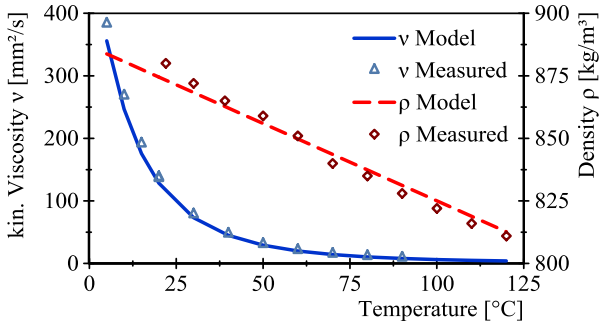

FIGURE 6. Viscosity and density of the hydraulic oil: Comparison of measured data and oil model

Solid Contact Calculation

For a physically based calculation of the solid contact, the FE-model is coupled with Person's theory of rubber friction and contact mechanics [22]. For simplicity we assume a constant coefficient of solid friction (μ = 0.8) in this study. In realty this coefficient does for example depend on the normal load and the relative velocity. Based on the power spectral density (PSD) C of a rough surface and the material data of the rubber, a physically based correlation of gap height h and the contact pressure p' can be derived (eq. 3) [23]:

$$h = \sqrt{\pi}\,\gamma \int_{q_0}^{q_1} dq\, q^2\, C(q)\, w(q) \int_{p'_c}^{\infty} dp' \frac{1}{p'} e^{-[w(q)\,p'/E^*]^2} \tag{3}$$

The correlation for the cylinder surfaces 2 and 3 is shown in figure 7. Due to the rougher surface of cylinder 3 (h_{rms} = 2 µm) compared to cylinder 2 (h_{rms} = 0.6 µm) the contact pressure is higher for an equal separation of the mating surfaces.

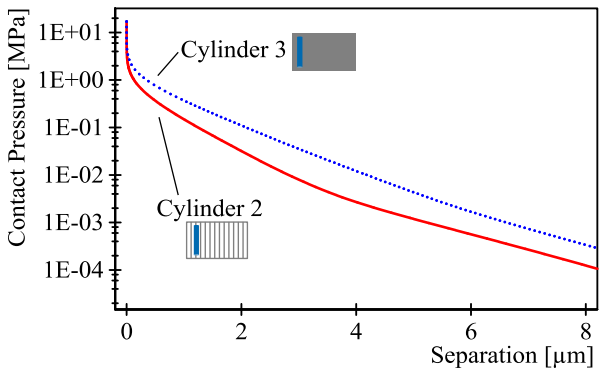

FIGURE 7. Contact pressure as a function of the separation for cylinders 2 and 3

SIMULATION RESULTS

In figure 8 the simulated heights of the sealing gap and the corresponding fluid pressures are shown for all three surfaces at different velocities. The results were carried out for a normal load of 31.1 N at a system temperature of 20 °C and a system pressure of 1 bar.

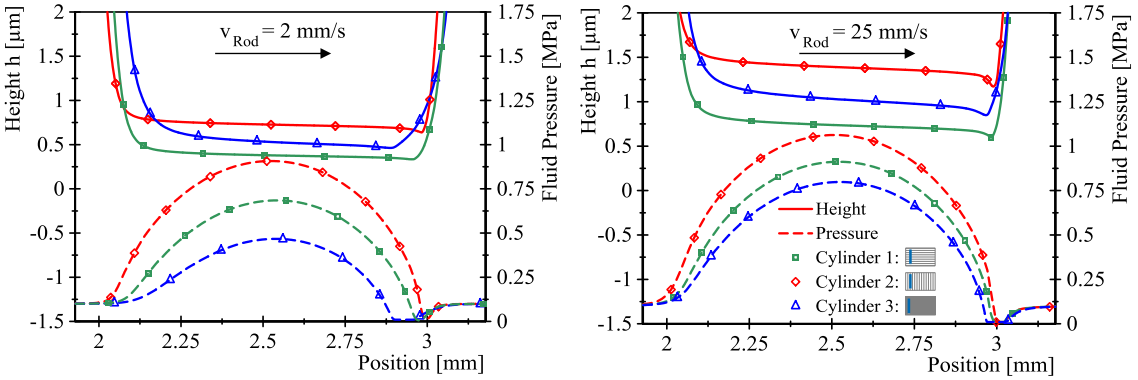

FIGURE 8. Simulation results: gap height h and fluid pressure p_{Fluid} for all three surfaces for two different relative velocities (normal load: 31.1 N)

For the simulation of cylinder 1 the same contact pressure distribution as for cylinder 2 was assumed (as the same manufacturing process was applied), only the flow factors were adjusted according to figure 5. Thus, the sole influence of the flow factors can be studied.
The surface structure of cylinder 2 leads to the highest fluid pressure, resulting in a higher gap height. Due to the different surface topography the fluid pressure is reduced for cylinder 1. Still, the fluid pressure is higher compared to the surface with isotropic roughness. This is caused by the smaller contact separation for cylinder 1. For cylinder 3 a higher amount of solid pressure already arises at larger gap heights (see figure 7). Thus, the amount of solid contact is increased, resulting in a larger sealing gap at lower fluid pressures.
In the cavitation regime a lower limit (vapour pressure) is implemented in order to avoid negative pressures.

EXPERIMENT AND COMPARISON

For the experimental investigations a test rig was designed, manufactured and set up at the Institute for Fluid Power Drives and Controls (IFAS) [2]. Steady sliding and accelerated sliding motions are studied. An O-ring specimen is squeezed in contact with a rotating rigid cylinder (Figure 9 a)). The experimental setup is summarised in table 1.

TABLE 1. Experimental Setup

Material of the O-ring	NBR 70 Shore A
Diameter of the O-ring	5 mm
Length of the specimen	40 mm
Normal load (normal force)	1 kg (31.1 N), 3 kg (63.3 N), 5 kg (155.5 N)
Temperature	5 °C, 20 °C, 40 °C (± 1°C)
Fluid	HLP 46

The experimental data is compared to simulation results in figures 9 b) – d). The shown experiments were performed at quasi stationary conditions (constant velocity for each measurement point, 20 °C, constant normal load). Therefore, the transient term of the Reynolds equation is neglected in the simulation for this part of the comparison.

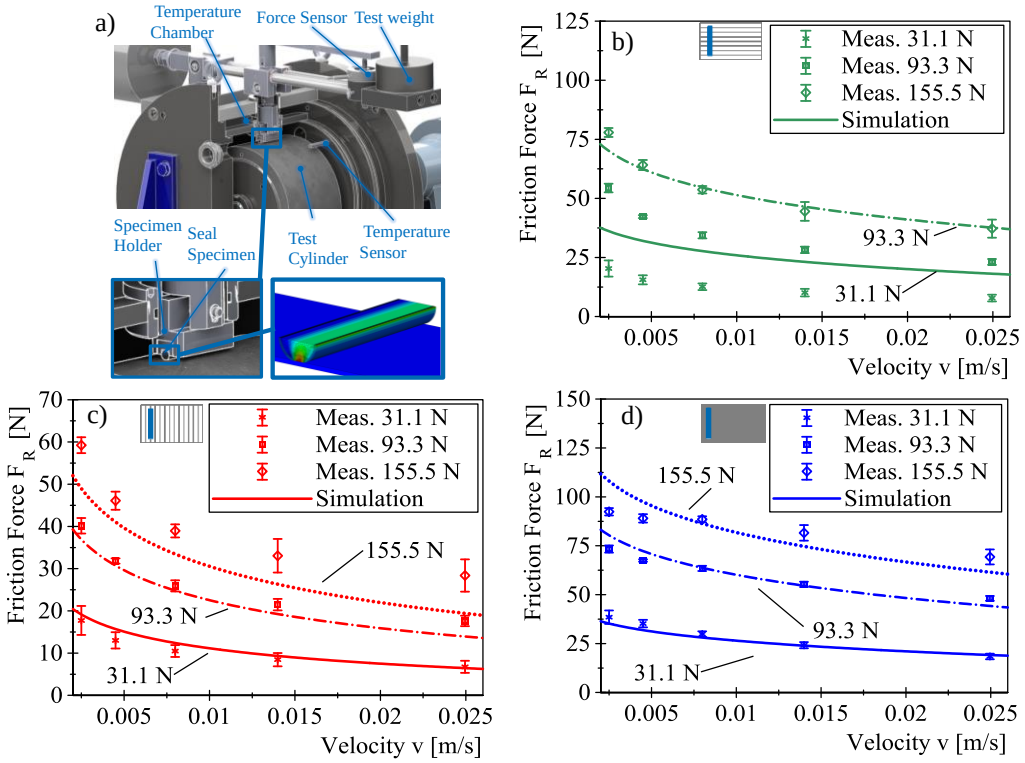

FIGURE 9. a) CAD picture of the test rig (detail of contact zone and corresponding FE model on the bottom) b) - d): Friction force as a function of the velocity (simulation and measurement) for three different normal loads (b) surface grooved in direction of motion , c) surface grooved orthogonal to direction of motion, d) isotropic rough surface)

As expected in the regime of mixed friction, the friction force declines when the velocity is increased. In experiment and simulation higher normal loads lead to higher friction forces. For cylinders 2 (c)) and 3 (d)) the results are in a good agreement, qualitatively as well as quantitatively. For cylinder 2 the simulated friction force at high normal loads is smaller, still the influence is in the correct order of magnitude. For cylinder 1 (b)) the simulated friction forces are higher, compared to the measurement. The simulated friction at a normal load of 93.3 N is similar to the measured force at 155.5 N. Thus, the assumption of a surface identical to cylinder 2 might be invalid. Still, the influence of the flow factors is correct. The friction forces are higher, when the surface is ground in the direction of motion.

A comparison for an accelerated motion is shown in figure 10. Here the transient term of the Reynolds equation is considered. Measurement and simulation were carried out for the cylinder with isotropic roughness. In simulation 1 the flow factors, and thus the influence of the surface topography, were neglected. In Simulation 2 the surface structure is considered. Two additional comparisons can be found in the appendix (figure 12).

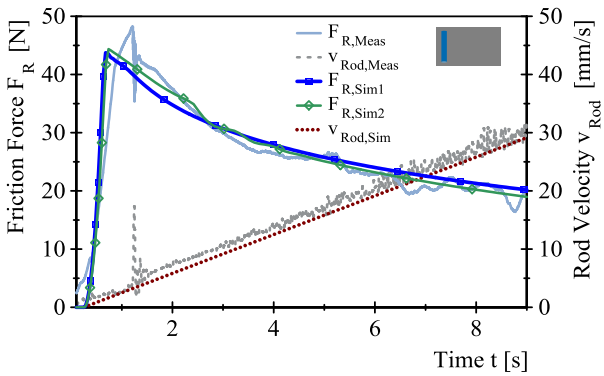

FIGURE 10. Comparison of simulation and measured friction force for a dynamic, accelerated motion

The influence of the surface structure is especially visible in the initial phase of motion (t ≈ 1-2 s) and for higher velocities (t > 5 s). In general simulation and measurement are in a good agreement. The maximum peak of friction (t > 1 s) is higher in the measurement. This might be caused by the velocity dependent tangential stress in the solid contact zone. Also the breakaway force is influenced by the idle time before starting the experiment.

Temperature Influence

On the left side in figure 11 the measured friction force (cylinder 2) is shown for three different temperatures at two different normal loads. The corresponding simulation is shown in the right figure.

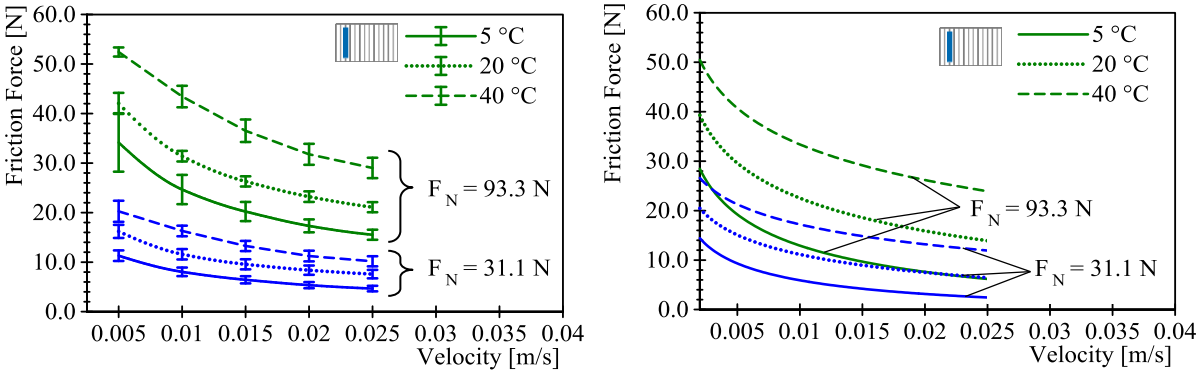

FIGURE 11. Friction force as a function of the velocity for two different normal loads and three different temperatures (left: measurement, right: simulation)

In both results, measurement and simulation, a higher temperature leads to higher friction forces. The simulated influence of the temperature is in the correct order of magnitude but more distinct, especially for the low temperature (5 °C). In the simulation the effect is mainly caused be the changing oil viscosity. For the examined system conditions a higher viscosity leads to higher simulated fluid pressures in the contact. Thus, solid contact and solid friction are reduced, leading to lower frictional stresses in the mixed friction regime. The simulated influence of the changing material properties can be neglected on the macroscopic scale for the investigated temperatures. The results shows, that a sole consideration of temperature depended oil viscosity on the macroscopic scale is not sufficient. An implementation of the microscopic temperature effects might lead to more accurate simulation results.

CONCLUSION

Different temperatures and surface structures have a considerable influence on the friction force of hydraulic seals. Both influences were implemented in a finite element (FE) based elastohydrodynamic (EHD) simulation for translational hydraulic seals. The simulation results were compared to experimental data of mixed friction force measurements, revealing a good qualitative and quantitative agreement. An implementation of a temperature and velocity depended micro contact model and normal contact data of cylinder 1 might lead to more accurate results.

ACKNOWLEDGMENTS

The research work was performed within a Reinhart-Koselleck project (DFG-Grant: MU 1225/36-1) funded by the Deutsche Forschungsgemeinschaft (DFG). The research work was also supported by the DFG-Grant: PE 807/10-1. We would like to thank DFG for the financial support.

REFERENCES

[1] G. K. Nikas, "Eighty years of research on hydraulic reciprocating seals," *Proceedings of the Institution of Mechanical Engineers, Part J: Journal of Engineering Tribology,* vol. 224, no. 1, p. 1–23, 2010.

[2] J. Angerhausen, H. Murrenhoff, L. Dorogin, M. Scaraggi, B. Lorenz and Persson, B. N. J., "Influence of anisotropic surfaces on the friction behaviour of hydraulic seals," *Proceeding of the 2016 Bath/ASME Symposium on Fluid Power and Motion Control,* 2016.

[3] F. Kaiser, B. Sauer and S. Eckert, "Development and Validation of a New Method for the Simulation of Starved Conditions of Rod Seals," *18th International Sealing Conference,* 2014.

[4] H. Blok, "Inverse problems in hydrodynamic lubrication and design directives for lubricated flexible surfaces," *Proceedings of the International Symposium on Lubrication and Wear, D. Muster and B. Sternlicht eds, Houston, USA,* p. 1–151, 1963.

[5] G. K. Nikas, "Elastohydrodynamics and Mechanics of Rectangular Elastomeric Seals for Reciprocating Piston Rods," *Journal of Tribology,* vol. 125, no. 1, p. 60, 2003.

[6] R. F. Salant, N. Maser and B. Yang, "Numerical Model of a Reciprocating Hydraulic Rod Seal," *Journal of Tribology,* vol. 129, no. 1, p. 91, 2007.

[7] X. Jia, S. Jung, W. Haas and R. F. Salant, "Numerical simulation and experimental study of shaft pumping by plunge ground shafts with rotary lip seals," *Tribology International,* vol. 48, p. 155–161, 2012.

[8] A. K. Bullock, D. G. Tilley, D. N. Johnston, C. R. Bowen and P. S. Keogh, "Non-linear friction in reciprocating hydraulic rod seals: Simulation and measurement," *Journal of Physics: Conference Series,* vol. 181, p. 012009, 2009.

[9] B. Yang and R. F. Salant, "Elastohydrodynamic lubrication simulation of O-ring and U-cup hydraulic seals," *Proceedings of the Institution of Mechanical Engineers, Part J: Journal of Engineering Tribology,* vol. 225, no. 7, p. 603–610, 2011.

[10] N. Patir and H. S. Cheng, "An Average Flow Model for Determining Effects of Three-Dimensional Roughness on Partial Hydrodynamic Lubrication," *Journal of Lubrication Technology,* vol. 100, no. 1, p. 12, 1978.

[11] Y. Huang and R. Salant, "Numerical Modelling of a Hydraulic Rod Seal with a Micro-Patterned Rod," *Proceedings of the 18th International Sealing Conference, Stuttgart,* pp. 611-623, 2014.

[12] A. N. Wohlers, O. Heipl and H. Murrenhoff, "Computational Study of the Influence of Roughness on the Friction Behaviour of Step Seals," *Proceedings : 6th FPNI - PhD Symposium West Lafayette 2010 ; West Lafayette, Indiana, USA, June, 15 - 19, 2010 ; an initiative of Fluid Power Net International / Ed. Monika Ivantysynova. - Vol. 1,* p. 363–372, 2010.

[13] A. N. Wohlers, O. Heipl, B. Persson, M. Scaraggi and H. Murrenhoff, "Numerical and Experimental Investigation on o-ring seals," *International Journal of Fluid Power,* 2009.

[14] Y. Öngün, M. Andre, D. Bartel and L. Deters, "An axisymmetric hydrodynamic interface element for finite-element computations of mixed lubrication in rubber seals," *PROCEEDINGS OF THE INSTITUTION OF MECHANICAL ENGINEERS PART J-JOURNAL OF ENGINEERING TRIBOLOGY,* vol. 222, no. J3, p. 471–481, 2008.

[15] Y. Öngün, "Finite element simulation of mixed lubrication of highly deformable elastomeric seals", Aachen: Shaker, 2010.

[16] T. Schmidt, "Mischreibung und Verschleiß in Hydraulikdichtsystemen," Gottfried Wilhelm Leibniz Universität, Hannover, 2011.

[17] J. Angerhausen, H. Murrenhoff, Persson, B. N. J., L. Dorogin and M. Scaraggi, "Finite Element based transient elastohydrodynamic simulation of transient hydraulic seals", submitted for review to: *International Journal of Fluid Power,* 2017.

[18] Dassault Systémes, ABAQUS (2016) ABAQUS Documentation, RI, USA, 2016.

[19] M. L. WILLIAMS, R. F. LANDEL and J. D. FERRY, "The Temperature Dependence of Relaxation Mechanisms in Amorphous Polymers and Other Glass-forming Liquids," *JOURNAL OF THE AMERICAN CHEMICAL SOCIETY,* vol. 77, no. 14, p. 3701–3707, 1955.

[20] M. Scaraggi, J. Angerhausen, L. Dorogin, H. Murrenhoff and B. Persson, "Influence of anisotropic surface roughness on lubricated rubber friction withapplication to hydraulic seals", submitted for review to: *Wear,* 2017.

[21] K. Witt, "Druckfluessigkeiten und thermodynamisches Messen", Frankfurt/M.: Ingenieur Digest Verlagsges, 1974, p. 190.

[22] Persson, B. N. J., "Theory of rubber friction and contact mechanics," *The Journal of Chemical Physics,* vol. 115, no. 8, p. 3840, 2001.

[23] B. Persson, "Relation between Interfacial Separation and Load: A General Theory of Contact Mechanics," *Physical Review Letters,* vol. 99, no. 12, 2007.

APPENDIX

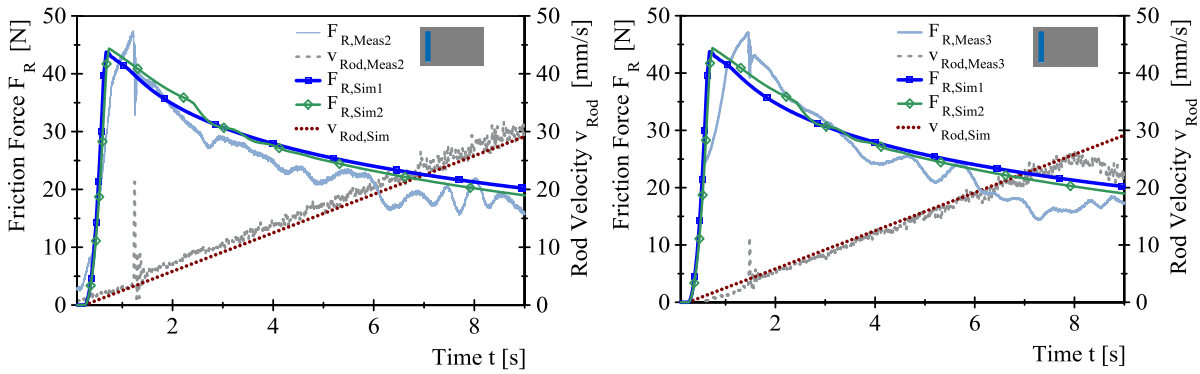

FIGURE 12. Comparison of simulation and measured friction force for a dynamic, accelerated motion (two additional measurement results)